Differential Equations for Morphological Amoebas

Martin Welk, Michael Breuß, and Oliver Vogel

Mathematical Image Analysis Group
Faculty of Mathematics and Computer Science, Campus E1.1
Saarland University, 66041 Saarbrücken, Germany
{welk,breuss,vogel}@mia.uni-saarland.de
http://www.mia.uni-saarland.de

Abstract. This paper is concerned with amoeba median filtering, a structure-adaptive morphological image filter. It has been introduced by Lerallut et al. in a discrete formulation. Experimental evidence shows that iterated amoeba median filtering leads to segmentation-like results that are similar to those obtained by self-snakes, an image filter based on a partial differential equation. We investigate this correspondence by analysing a space-continuous formulation of iterated median filtering. We prove that in the limit of vanishing radius of the structuring elements, iterated amoeba median filtering indeed approximates a partial differential equation related to self-snakes and the well-known (mean) curvature motion equation. We present experiments with discrete iterated amoeba median filtering that confirm qualitative and quantitative predictions of our analysis.

Keywords: morphological amoebas, median filtering, partial differential equations.

1 Introduction

Morphological amoebas are a class of morphological image filters in which structuring elements adapt to image structures with a maximum of flexibility. They have been introduced by Lerallut et al. [11,12]. In the amoeba construction, the structuring elements adapt locally to the variation of grey (or colour) values, also taking into account the distance to the origin pixel. Thereby, large deviations in the image values are penalised, so that the amoebas may grow around corners or along anisotropic image structures. Using the resulting shape as a structuring element, many filtering procedures can be applied on it. In this paper, we are particularly interested in the use of the median filter.

Iterated application of amoeba median filtering (AMF) can be carried out in different ways. In [11], a *pilot image* is used to steer the iterated processes via an alternating procedure. This works as follows. A smoothed version of the original image f is used for constructing amoebas for all pixels. Then, the median filter is applied using the corresponding structuring elements. The filtered image is

M.H.F. Wilkinson and J.B.T.M. Roerdink (Eds.): ISMM 2009, LNCS 5720, pp. 104–114, 2009.
© Springer-Verlag Berlin Heidelberg 2009

in turn used for constructing new amoebas, and these amoebas are then used as structuring elements to filter the original image f. We concentrate for this paper on more straightforward iterative procedures for AMF, using pixelwise the following steps subsequently: (i) amoeba construction, and (ii) median filtering using the amoeba as structuring element.

For iterated median filtering with a fixed structuring element, work by Guichard and Morel [7] has brought out that, in the continuous-scale limit, it approximates the *partial differential equation (PDE)* $u_t = |\nabla u| \operatorname{div}\big(\nabla u / |\nabla u|\big)$, known as (mean) curvature motion [1]. In this sense, iterated discrete median filtering with a fixed structuring element can be understood as a specific discretisation of that PDE.

Iterated AMF simplifies images towards a cartoon-like appearance with homogeneous regions separated by sharp contours. Even corners are preserved fairly well, in contrast to median filtering with a fixed structuring element. Using PDE approaches, similar segmentations can be achieved e.g. by so-called self-snakes [14,18]. These are filters that stand in close relationship to curvature motion, with the difference that the evolution is modulated by an edge-stopping function depending on the local image gradient. Thereby the displacement of edges is avoided, and edges are sharpened. In the light of Guichard and Morel's above-mentioned result it is therefore natural to ask whether there exists a similar correspondence between a continuous-scale limit case of amoeba filters and a self-snakes-like PDE.

In the present paper, we address this question. We prove that iterated amoeba filtering can indeed be understood as a discrete approximation of a PDE which is related to curvature motion. We discuss how different choices for the distance measures involved in the amoeba definition influence the limit case.

Our results extend the framework of known correspondences between discrete and PDE formulations of morphological filters. The study of these relationships helps to gain a unified view on image filtering methods and to combine advantages of both approaches.

Related work. Median filtering in its non-adaptive form goes back to Tukey [16] and became common as a structure-preserving image filter in the 90s [6,9].

On the PDE side, (mean) curvature motion for image smoothing has been proposed by Alvarez et al. [1], already together with the generalisation of the basic PDE by multiplying the right-hand side with a decreasing function of the image gradient. Sapiro [14] proposed a variant of this idea, named self-snakes, in which the edge-stopping factor is placed *within* the divergence expression. While curvature motion smoothes in level-line direction only, Caselles et al. [3] defined for image interpolation purposes a process that smoothes exclusively in gradient direction, called *adaptive monotone Lipschitz extension* (AMLE). The representation of an image as a manifold embedded in the product space of image domain and greyvalue range has been introduced in PDE-based image filtering with the so-called Beltrami framework by Kimmel et al. [8] and Yezzi [19].

Since the seminal paper by Guichard and Morel [7] further cross-relationships between discrete and PDE-based image filters have been studied. For example,

van den Boomgaard [17] proved a PDE approximation result for the Kuwahara-Nagao operator [10,13]. Didas and Weickert [5] studied correspondences between adaptive averaging and a class of generalised curvature motion filters. Barash [2] and Chui and Wang [4] considered PDE limits of bilateral filters [15].

Structure of the paper. The paper is organised as follows. In Section 2 we describe the discrete algorithm. Our main contribution, namely the derivation of a PDE corresponding to AMF, follows in Section 3. In Section 4, we show some test results. The paper is finished with a conclusion in Section 5.

2 The Discrete Amoeba Construction

The basic procedure is described in Lerallut et al.'s papers [11,12]. Here, we give a brief account of the algorithm in the form we have implemented, which is slightly modified in a few points that will be pointed out in the sequel.

In the following, we work with images f whose pixels are numbered by integers, such that f_i denotes the grey value of the pixel with index i. The coordinates of this pixel are denoted by (x_i, y_i). We distinguish the initial image f from the iterated images $u^{(n)}$, where n denotes the iteration number. For starting the iterative process, we set $u^{(0)} := f$. On the amoebas whose construction is described below the standard median filter is applied.

Description of the algorithm. For each pixel i_0 with (x, y)-coordinates (x_{i_0}, y_{i_0}), an adaptive structuring element is determined as follows. We consider pixels i^* within a prescribed maximal Euclidean distance ϱ of pixel i_0. The number ϱ represents the maximal size of the shape of the amoeba, since it will also be used for limiting the allowed *amoeba distance*. For the so pre-selected pixels we consider paths $(i_0, i_1, \ldots, i_k \equiv i^*)$ that connect i_0 with i^* via a sequence of pixels in which each two subsequent pixels i_j, i_{j+1} are neighbours. Among all these, we determine the shortest path P with respect to the amoeba distance $L(P)$. If the amoeba distance is below ϱ for P, the pixel i^* is accepted as a member of the amoeba structuring element.

It remains to specify the amoeba distance as well as the neighbourhood relation between subsequent pixels. In [11,12], the amoeba distance is given by

$$L_L^{(n)}(P) \;=\; \sum_{m=0}^{k-1} 1 + \sigma \sum_{m=0}^{k-1} \left| u_{i_{m+1}}^{(n)} - u_{i_m}^{(n)} \right| \,, \tag{1}$$

where $\sigma > 0$ is a parameter that penalises large deviations in grey value data, and each pixel is required to be in the 4-neighbourhood of its predecessor, i.e. a horizontal or vertical neighbour. Note that this definition involves the measurement of spatial distances by the city-block metric, since the first sum in (1) counts the pixels in the path P (without the starting pixel i_0). Moreover, spatial and tonal distances (i.e. greyvalue differences) are combined via an l_1 sum.

In our implementation, we use a metric that better approximates the Euclidean distance in space. To this end, we use 8-neighbourhoods that include

horizontal, vertical, and diagonal neighbours, and use the Euclidean distance on these pixel pairs. This results in shorter paths compared to the procedure of Lerallut et al., as well, conceptually, in an improvement in terms of rotational invariance. For the way how spatial and tonal distances are combined we consider either a Euclidean sum, or an l_1 sum like in (1), which leads finally to two alternative amoeba distance measures L_2 and L_1 given by

$$L_2^{(n)}(P) = \sum_{m=0}^{k-1} \sqrt{\left(x_{i_{m+1}} - x_{i_m}\right)^2 + \left(y_{i_{m+1}} - y_{i_m}\right)^2 + \sigma^2 \left(u_{i_{m+1}}^{(n)} - u_{i_m}^{(n)}\right)^2}, \quad (2)$$

$$L_1^{(n)}(P) = \sum_{m=0}^{k-1} \left(\sqrt{\left(x_{i_{m+1}} - x_{i_m}\right)^2 + \left(y_{i_{m+1}} - y_{i_m}\right)^2} + \sigma \left| u_{i_{m+1}}^{(n)} - u_{i_m}^{(n)} \right| \right) . \quad (3)$$

3 Space-Continuous Analysis

For our further investigation, we need a space-continuous formulation of AMF. We base this on the representation of a (smooth) image u by its graph $\Gamma = \Gamma_{u,\sigma} := \{p(x,y) = (x,y,\sigma u(x)) \mid (x,y) \in \Omega\}$ where $\Omega \subset \mathbb{R}^2$ is the image domain, and σ a scaling parameter for grey-values as in (1)–(3). Note that this embedding is analogous to the Beltrami framework, compare [19]. The surface Γ is equipped with a metric d which can be obtained by restricting the Euclidean metric of the embedding space $\mathbb{R}^3$, i.e.

$$d(p_1,p_2) \equiv d_2(p_1,p_2) = \min \int_0^1 \sqrt{x'(s)^2 + y'(s)^2 + \sigma^2 u'(s)^2}\, \mathrm{d}s \quad (4)$$

where the minimum is taken over all curves $[0,1] \to \Gamma$ that start in $p_1 := p(x_1,y_1)$ and end in $p_2 := p(x_2,y_2)$. Alternatively, and closer to the setting of [11], one can use an l_1 sum of the Euclidean distance in space and the greyvalue distance,

$$d(p_1,p_2) \equiv d_1(p_1,p_2) = \min \int_0^1 \left(\sqrt{x'(s)^2 + y'(s)^2} + \sigma \left| u'(s) \right| \right) \mathrm{d}s \, . \quad (5)$$

One step of amoeba filtering then reads as follows. For a given location (x_0,y_0) in the image domain, an amoeba structuring element $\mathcal{A}(x_0,y_0)$ is constituted by all locations (x,y) for which $d(p(x_0,y_0),p(x,y))$ does not exceed a given radius ϱ. Typical shapes of amoeba structuring elements with both metrics are shown in Figure 1. It is worth noticing that with the metric (4) the boundary of $\mathcal{A}(x_0,y_0)$ crosses the level line through (x_0,y_0) orthogonally and smoothly, while with (5) it has kinks at the intersection points, giving the structuring element a digonal overall shape in contrast to the elliptical contour with (4).

Once the structuring element has been constructed, the median of all grey-values within the structuring element is taken, i.e. the value μ whose level line

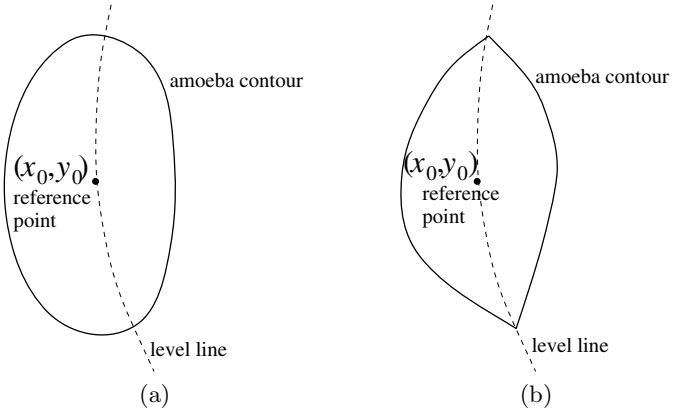

Fig. 1. Amoeba structuring elements. **(a)** Typical amoeba with metric $d \equiv d_2$ from (4). **(b)** Typical amoeba with metric $d \equiv d_1$ from (5).

(the curve along which $u(x, y) = \mu$ holds) cuts $\mathcal{A}(x_0, y_0)$ into two parts of equal area. In the filtered image, μ becomes the new grey-value at location (x_0, y_0).

We analyse this filter now in a manner similar to Guichard and Morel's approach [7]. We focus first on the case of the metric $d \equiv d_2$, see (4). Without loss of generality, we assume that we are dealing with the location $(x_0, y_0) = (0, 0)$. We assume further that $u(x_0, y_0) = 0$, and that the image gradient at (x_0, y_0) is given by $\nabla u(x_0, y_0) = (\alpha/\sigma, 0)^{\mathrm{T}}$ with some positive α. Then σu possesses the Taylor expansion

$$\sigma u(x, y) = \alpha x + \beta x^2 + \gamma xy + \delta y^2 + \mathcal{O}(\varrho^3) \tag{6}$$

within $\mathcal{A} = \mathcal{A}(x_0, y_0)$, where we have used that $x, y = \mathcal{O}(\varrho)$.

Consider now a value $z = \mathcal{O}(\varrho)$. We are interested in the level line of u corresponding to the grey-value z/σ, restricted to $\mathcal{A}$. On this line, $\sigma u(x, y) = z$ holds. Due to the prescribed gradient direction of u, level lines of u within $\mathcal{A}$ are roughly oriented in y direction. We can therefore express the level line by writing x as a function of y. Resolving the equation $\sigma u(x) = z$ for x yields

$$x = x(y) = \left(\frac{z}{\alpha} - \frac{z^2\beta}{\alpha^3}\right) - \frac{z\gamma}{\alpha^2}y - \frac{\delta}{\alpha}y^2 + \mathcal{O}(\varrho^3)\,. \tag{7}$$

(As a quadratic equation needs to be solved, there is a second solution which is, however, outside $\mathcal{A}$ if ϱ is small enough.) The length of the level line segment within $\mathcal{A}$ acts as a weight with which the value $u = z/\sigma$ enters the computation of the median μ. The end points of this segment are obtained by equating $d_2(p(x_0, y_0), p(x(y), y))$ to ϱ. Approximating d_2 by the Euclidean distance within $\mathbb{R}^3$, this equation becomes $x(y)^2 + y^2 + z^2 = \varrho^2$, a quadratic equation for y with two solutions y_1, y_2. The length $L(z)$ of the level line segment within $\mathcal{A}$ equals up to $\mathcal{O}(\varrho^3)$ the difference $|y_1 - y_2|$. We compute therefore

$$L(z) = 2\varrho\sqrt{1 - \frac{z^2(\alpha^2+1)}{\varrho^2\alpha^2}}\left(1 + \frac{z\delta}{\alpha^2} + \frac{z^3\beta}{\alpha^2\left(\alpha^2\varrho^2 - z^2(\alpha^2+1)\right)}\right) + \mathcal{O}(\varrho^3)\ . \quad (8)$$

The median μ is now determined by the equality

$$\int_{Z_-}^{\sigma\mu} L(z)\,\mathrm{d}z = \int_{\sigma\mu}^{Z_+} L(z)\,\mathrm{d}z\ , \quad (9)$$

where Z_+ and Z_- are the smallest positive and largest negative values for which $L(Z_+) = L(Z_-) = 0$. One has $Z_+, Z_- = Z^* + \mathcal{O}(\varrho^3)$ with $Z^* = \varrho\alpha/\sqrt{\alpha^2+1}$. Provided that $\mu = \mathcal{O}(\varrho^2)$, the equality (9) can be transformed into

$$\int_0^{Z^*} (L(z) - L(-z))\,\mathrm{d}z = 2\sigma\mu L(0) + \mathcal{O}(\varrho^4)\ . \quad (10)$$

Resolving the integral on the left-hand side analytically yields $\frac{4\varrho^3\delta}{3(\alpha^2+1)} + \frac{8\varrho^3\beta}{3(\alpha^2+1)^2}$. Together with $L(0) = 2\varrho + \mathcal{O}(\varrho^3)$, this implies

$$\mu = \frac{\varrho^2}{3\sigma}\left(\frac{\delta}{\alpha^2+1} + \frac{2\beta}{(\alpha^2+1)^2}\right) + \mathcal{O}(\varrho^3) \quad (11)$$

which can be restated in terms of spatial derivatives of u as

$$\mu = \frac{\varrho^2}{6}\left(\frac{u_{yy}}{1+\sigma^2u_x^2} + \frac{2u_{xx}}{(1+\sigma^2u_x^2)^2} + \mathcal{O}(\varrho)\right)\ . \quad (12)$$

One amoeba median filter step acts therefore approximately like one time step of an explicit scheme for the PDE

$$u_t = \frac{u_{\xi\xi}}{1+\sigma^2\left|\nabla u\right|^2} + \frac{2u_{\eta\eta}}{\left(1+\sigma^2\left|\nabla u\right|^2\right)^2} \quad (13)$$

with time step size $\tau = \varrho^2/6$. On the right-hand side, second derivatives are taken in the directions of the normalised gradient vector $\eta := \nabla u/\left|\nabla u\right|$ and the perpendicular vector $\xi := \eta^\perp$, the tangential vector of the local level line of u.

When ϱ tends to zero, the iterated amoeba median filter therefore converges to the PDE (13). The first summand of the right-hand side of (13) can obviously be interpreted as curvature motion $u_t = u_{\eta\eta}$ modulated in the way proposed in [1] by an edge-stopping factor $g_1(|\nabla u|) := \left(1+\sigma^2\left|\nabla u\right|^2\right)^{-1}$. It can also be compared to the self-snakes PDE [14,18]

$$u_t = |\nabla u|\,\mathrm{div}\left(g(|\nabla u|)\frac{\nabla u}{|\nabla u|}\right) = g(|\nabla u|)u_{\xi\xi} + \langle\nabla g(|\nabla u|), \nabla u\rangle\ , \quad (14)$$

except that the term $\langle\nabla g, \nabla u\rangle$ is not present. As this "shock term" contributes to the edge-enhancing properties of the self-snakes evolution, the edge-enhancing effect may be less pronounced with the amoeba filter than with self-snakes.

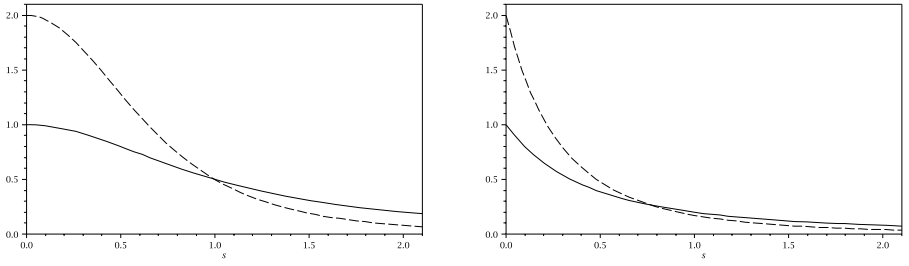

(a) (b)

Fig. 2. Edge-stopping functions in PDEs approximated by iterated amoeba median filtering. For visualisation, σ is fixed to 1. **(a)** Weight functions $g_1 = \big(1+|\nabla u|^2\big)^{-1}$ for the curvature motion term (solid line), $g_2 = 2\big(1+|\nabla u|^2\big)^{-2}$ for the AMLE term (dashed line) from the PDE (13) based on the Euclidean amoeba metric (4). **(b)** Corresponding weight functions for the amoeba metric (5).

The second summand of (13) resembles the AMLE [3] evolution $u_t = u_{\eta\eta}$, but with an edge-stopping factor $g_2(|\nabla u|) := 2\big(1 + \sigma^2\,|\nabla u|^2\big)^{-2}$. Note that g_2 decreases faster than g_1, with $g_1 = g_2$ for $|\nabla u| = \sigma^{-1}$, see Figure 2 (a). At all locations where the gradient is sufficiently large, the PDE (13) is therefore dominated by the self-snakes-like modulated curvature motion part. The AMLE contribution dominates in almost flat image regions.

A similar analysis applies if instead of d_2 the metric d_1 from (5) is used. The resulting equation is again of the form $u_t = g_1(|\nabla u|)u_{\xi\xi} + g_2(|\nabla u|)u_{\eta\eta}$ with decreasing functions g_1, g_2 of the gradient. Here, g_1 and g_2 are given by complicated integral expressions that are best evaluated numerically, see Figure 2 (b). The derivation for this case will be published in a forthcoming paper.

4 Experiments

We present two experiments that confirm the behaviour suggested by the analytical results from the previous section.

The *House* experiment. In this experiment we use a relatively "simple" image in order to investigate the influence of parameters, see Figure 3.

Subfigure (a) shows the original image. Figure 3(b) depicts the steady state achieved by standard median filtering employing a fixed (3×3) structuring element. As usual with median filtering, the shape of edges is rounded, and the facade of the depicted house is quite non-uniform in its grey value distribution. The use of a larger non-adaptive structuring element will distort the shape of important image features.

In Figure 3(c–f) we compare the results of iterated AMF using the L_2 amoeba distance together with varying parameters.

We start with a relatively strong penalisation of grey value differences given by $\sigma = 0.25$, see (c, d). As predicted, we observe the influence of the self-snakes

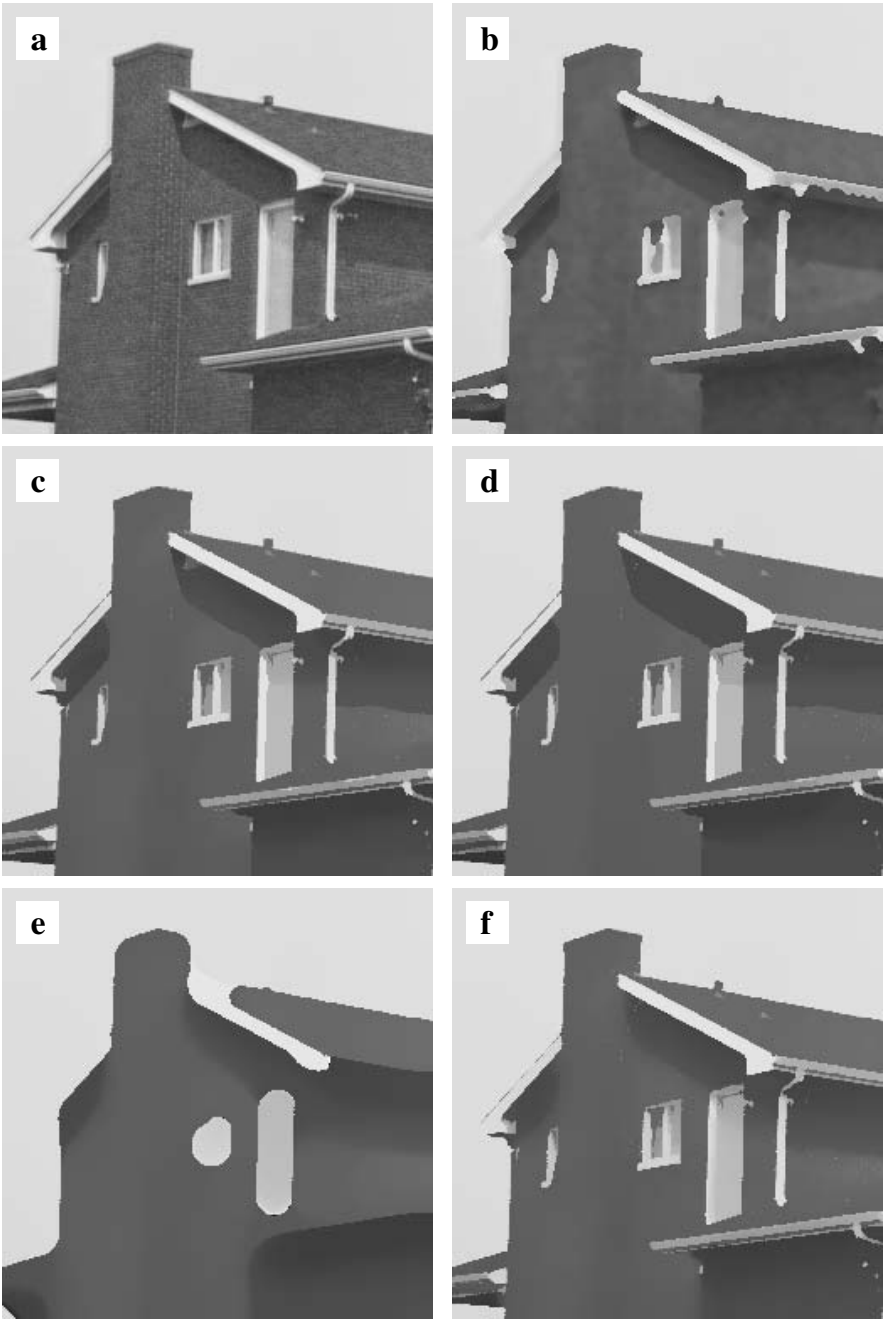

Fig. 3. The *House* experiment. **Top row: (a)** Original image. **(b)** Filtered with iterated median filter, 3×3 stencil, 40 iterations. **Middle row: (c)** Iterated AMF, $\varrho = 10$, $\sigma = 0.25$, 4 iterations. **(d)** Same as in (c) but 20 iterations. **Bottom row: (e)** Iterated AMF, $\varrho = 10$, $\sigma = 0.02$, 10 iterations. **(f)** Iterated AMF, $\varrho = 20$, $\sigma = 0.25$, 1 iteration.

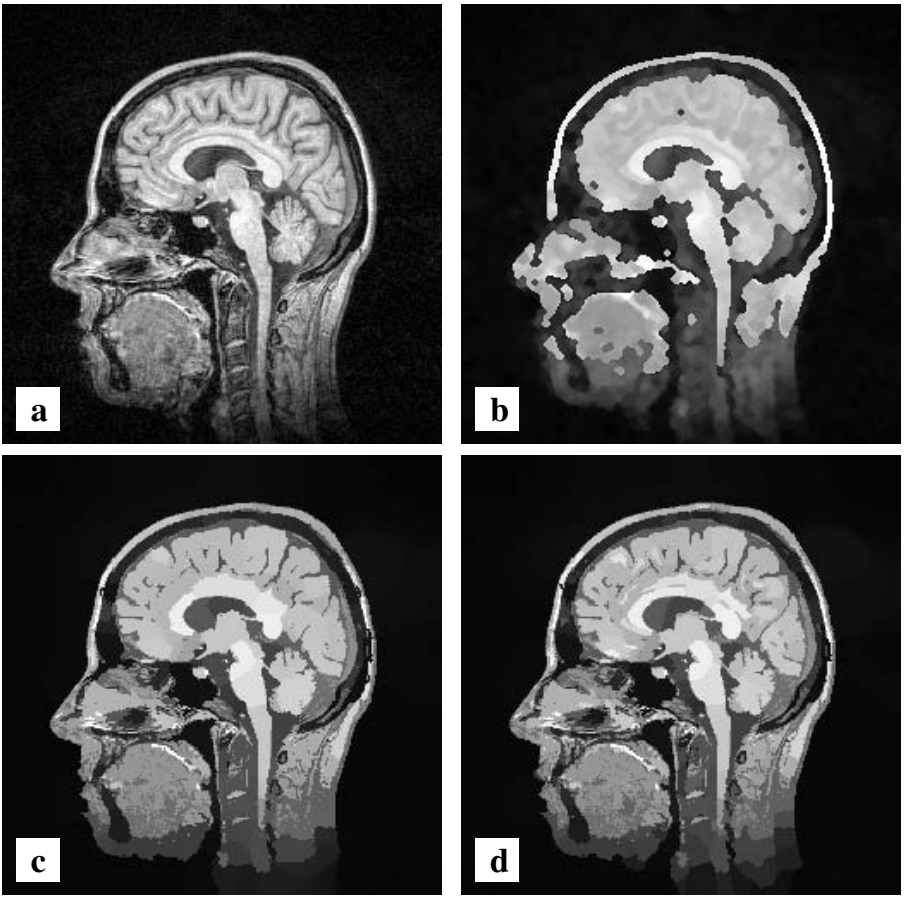

Fig. 4. The *Head* experiment. **Top row: (a)** Original image. **(b)** Steady state of iterated median filter. **Bottom row: (c)** Iterated AMF, $\varrho = 10$, $\sigma = 0.25$, 10 iterations, L_2 amoeba distance. **(d)** Same but with L_1 amoeba distance.

very clearly by the sharp transition of regions of different grey values, while nearly flat image regions are flattened even more.

When a very small σ is used, as in Figure 3(e), the size of regions that are treated as nearly flat increases significantly. Indeed, we observe the corresponding dominant blurring-like influence of AMLE.

In Figure 3(f) we increase the amoeba parameter ϱ relative to the setting from (c, d). From the analytic point of view, this corresponds to a larger time step size: Due to the quadratic relationship $\tau = \varrho^2/6$ we can expect that for two structuring elements with radii ϱ_1 and $\varrho_2 = 2\varrho_1$, four AMF iterations with ϱ_1 should roughly make up one iteration with ϱ_2. The comparison of Figure 3(c) and (f) confirms this approximate relationship: One iteration with $\varrho = 20$ has a similar outcome as four iterations with $\varrho = 10$. We observe especially that the

transition zones at the shadows are located very similarly. The self-snake-like sharpening, however, appears somewhat more prominent in the image processed with four iterations.

The *Head* experiment. In this experiment (Figure 4) we use an MR image of a human head which is rich in details of different contrast and scale. The original image is shown in Subfigure (a). In (b–d) iterated AMF results both with L_2 and L_1 amoeba distance are displayed. It can be seen that both distance measures lead to similar results. Moreover, we observe even clearer than in the *House* experiment the good quality of segmentation that is achieved in spite of the relative simplicity of the filtering approach.

5 Conclusion

Our analysis of iterated amoeba median filtering shows that even highly adaptive discrete image filters can be interpreted in terms of PDE-based evolutions. This viewpoint leads to clear explanations of qualitative properties of iterated AMF, and predictions that can be confirmed by experiments. At the same time, the cross-relation sheds new light on well-known PDE filters and may inspire the development of new discretisations of PDE filters. Continuing this direction of research, we believe that it will not only expedite the development of both classes of image filters, but also bring forward a fusion between formerly distinct branches of image processing.

References

1. Alvarez, L., Lions, P.-L., Morel, J.-M.: Image selective smoothing and edge detection by nonlinear diffusion. II. SIAM Journal on Numerical Analysis 29, 845–866 (1992)
2. Barash, D.: Bilateral filtering and anisotropic diffusion: towards a unified viewpoint. In: Kerckhove, M. (ed.) Scale-Space 2001. LNCS, vol. 2106, pp. 273–280. Springer, Heidelberg (2001)
3. Caselles, V., Morel, J.-M., Sbert, C.: An axiomatic approach to image interpolation. IEEE Trans. Image Proc. 7(3), 376–386 (1998)
4. Chui, C.K., Wang, J.: PDE models associated with the bilateral filter. Advances in Computational Mathematics (2008)
5. Didas, S., Weickert, J.: Combining curvature motion and edge-preserving denoising. In: Sgallari, F., Murli, F., Paragios, N. (eds.) SSVM 2007. LNCS, vol. 4485, pp. 568–579. Springer, Heidelberg (2007)
6. Dougherty, E.R., Astola, J. (eds.): Nonlinear Filters for Image Processing. SPIE Press, Bellingham (1999)
7. Guichard, F., Morel, J.-M.: Partial differential equations and image iterative filtering. In: Duff, I.S., Watson, G.A. (eds.) The State of the Art in Numerical Analysis, pp. 525–562. Clarendon Press, Oxford (1997)
8. Kimmel, R., Sochen, N., Malladi, R.: Images as embedding maps and minimal surfaces: movies, color, and volumetric medical images. In: Proc. 1997 IEEE Computer Society Conference on Computer Vision and Pattern Recognition, pp. 350–355 (1997)

9. Klette, R., Zamperoni, P.: Handbook of Image Processing Operators. Wiley, New York (1996)
10. Kuwahara, M., Hachimura, K., Eiho, S., Kinoshita, M.: Processing of RI-angiocardiographic images. In: Preston, J.K., Onoe, M. (eds.) Digital Processing of Biomedical Images, pp. 187–202. Plenum, New York (1976)
11. Lerallut, R., Decencière, E., Meyer, F.: Image processing using morphological amoebas. In: Ronse, C., Najman, L., Decencière, E. (eds.) Mathematical Morphology: 40 Years On, pp. 13–22. Springer, Dordrecht (2005)
12. Lerallut, R., Decencière, E., Meyer, F.: Image filtering using morphological amoebas. Image and Vision Computing 25(4), 395–404 (2007)
13. Nagao, M., Matsuyama, T.: Edge preserving smoothing. Computer Graphics and Image Processing 9(4), 394–407 (1979)
14. Sapiro, G.: Vector (self) snakes: a geometric framework for color, texture and multiscale image segmentation. In: Proc. IEEE International Conference on Image Processing 1996, vol. 1, pp. 817–820 (1996)
15. Tomasi, C., Manduchi, R.: Bilateral filtering for gray and color images. In: Proc. Sixth International Conference on Computer Vision, pp. 839–846. Narosa Publishing House (1998)
16. Tukey, J.W.: Exploratory Data Analysis. Addison–Wesley, Menlo Park (1971)
17. Van den Boomgaard, R.: Decomposition of the Kuwahara–Nagao operator in terms of linear smoothing and morphological sharpening. In: Mathematical Morphology: Proc. Sixth International Symposium, pp. 283–292. CSIRO Publishing (2002)
18. Whitaker, R.T., Xue, X.: Variable-conductance, level-set curvature for image denoising. In: Proc. IEEE International Conference on Image Processing 2001, pp. 142–145 (2001)
19. Yezzi Jr., A.: Modified curvature motion for image smoothing and enhancement. IEEE Trans. Image Proc. 7(3), 345–352 (1998)